Supplementary

S1. Meteorology and cloud presence at Cimone

Here we present the meteorological conditions recorded at CMN in the 2007-2023 period. CMN experience a seasonal temperature seasonal cycle with a cold winter and temperate summer. Monthly averaged temperature increases from -2.7°C in January to 12.5°C in July (Figure S1a), with extreme daily mean between -15.4°C and 23.8°C. The overall RH median was 85%, following a seasonal cycle with most dry condition between July and August (monthly median RH below 75%) and more wet conditions during the rest of the year, with maximum monthly median observed in November (RH>95%). The ambient pressure increased from winter to summer following the temperature seasonality, showing an increase of approximately 10 hPa from January to August. Similar to Cristofanelli et al. (2018), winds from north-east (Po-Valley) and south-west (Tyrrhenian Sea) dominated the wind pattern since 2007 to 2023, while in T and RH did not show any statistically significant as function of wind direction. We assessed the presence of clouds using as a proxy the dew-point temperature. The dew point temperature (T_D) had a well-defined seasonal cycle (Figure S1a), characterized by a minimum of -6.0°C in January and maximum of 7.0°C in July. The interquartile ranges of T_A and T_D overlapped suggesting the occurrence of favourable conditions for condensation and frost during the whole year.

Cloud presence was derived from the dew point temperature (T_D). As summarized by Lawrence (2005), various approaches may be used to derive T_D in different temperature and RH regimes. We used the formula and relative constants (A1 = 17.625, B1 = 243.04°C, and C1 = 610.94 Pa) proposed by Alduchov and Eskridge (1996), which provides T_D values with a relative error below 0.4% in the CMN temperature range ($-15°C < T_A < 24°C$). We defined a decisional tree to identify and classify the potential cloud cases as function of the hourly variability of T_D (Figure S2a). A day was characterized by 24 hours of $T_A > (T_D + 1°C)$ was considered as "Cloud-free day". Vice-versa, a full day was defined as a "Cloud day" if T_A fell within 1°C from T_D ($T_D \leq T_A \leq (T_D + 1°C)$) for at least 1 hour. Moreover, if the number of hours respecting the before-described conditions of temperature were respected for less than 16 hours, the day was considered as a "Transient cloud day". Vice versa, if the condensation condition was respected for the entire day (24 h), the day was considered "Persistend cloud day". The cloud days where subsequently classified as function of the T_A sign as: full condensation (T_A above zero for 24 hours per day); mixed – dominated by condensation (T_A above zero between 12 and 23 hours per day); mixed – dominated by frost (T_A below zero between 12 and 23 hours per day); full frost (T_A below zero for 24 hours per day).

Overall, cloud conditions were observed 50% of the time along all years from 2007 to 2023 (Figure S2), with the highest fraction of cloud in spring and autumn (70% of cloudy days) and the lowest frequency (47%) in July and August. In the summer months, most cloud days were transient, with cloud condition lasting less than 16 hour per day (Figure S2b). On the other end, the fraction of persistent cloud days remained firmly above 50% from October to May. Among these persistent cloud days, the relative dominance of condensation and frost conditions changed from fully condensing conditions in summer (100% June-August) to mixed conditions in the winter months, when fully freezing conditions occurred between 67% and 80% of days per month from December to February (Figure S2c). This classification is important to investigate the impact of humidity on absorption measurements performed with filter-based observations and the efficiency of the inlet setup in de-humidifying the sampled air.

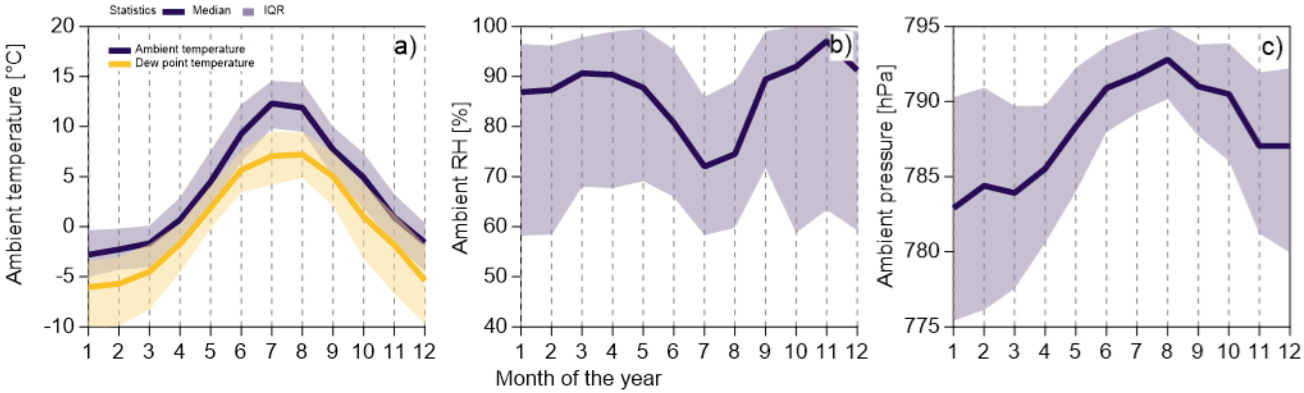

Figure S1 Monthly variability of meteorological parameters at CMN: a) Ambient and dew point temperature; b) ambient relative humidity; c) ambient pressure. Statistic calculated based observations at CMN between 2007 and 2023.

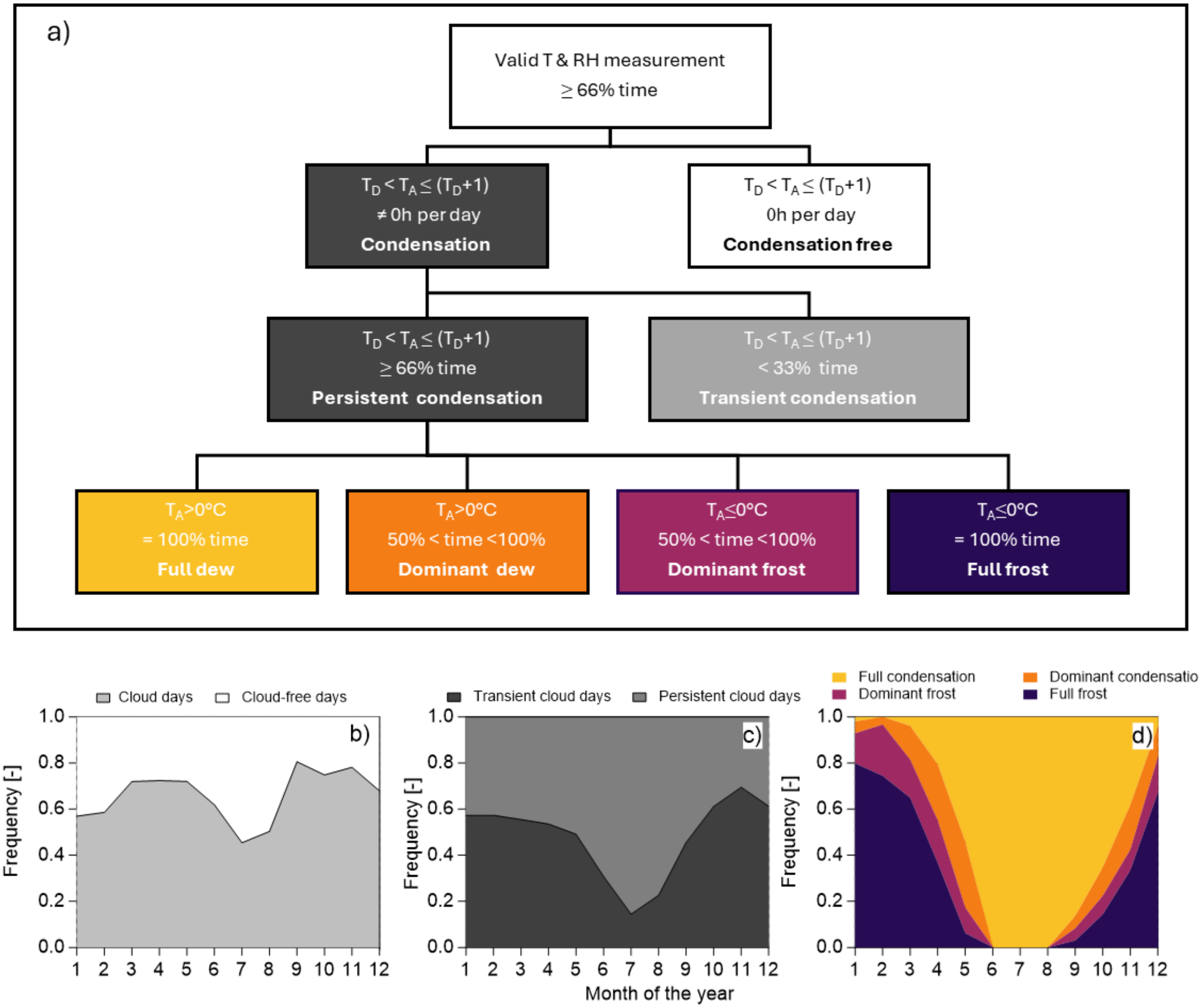

Figure S2 a) Characterization of cloud condition at CMN between 2007-2023. Decision tree schematics for the classification of cloud-free and cloud days, transient and persistent cloud days, and cloud types. Frequency of occurrence of: b) cloud-free and cloud days; c) transient and persistent cloud days; d) cloud phase (full condensation, dominant condensation, dominant frost, full frost). Statistic and cloud classes calculated based on ambient temperature and dew point temperature.

S2. Warming and drying inside the sampling line

We address the variability of the conditions inside the sampling line as a function of the various setups described before and compare it with atmospheric conditions. It was, however, impossible to directly compare the different inlet designs with the same sensors and compare the different sensors with the same inlet design. We thus calculated the difference between the temperature at the end of the sampling line and the ambient dew point temperature (ΔT), and the difference between the relative humidity at the end of the sampling line and the ambient relative humidity (ΔRH) on hourly base. The resulting cumulative histograms are shown in Figure S3. Even though the overall mean ΔT was 20.5 K (median value), a net change in ΔT was observed only after the upgrade to WAI-2. In fact, across Period A, B and C, the mean ΔT varied between 19.5 K and 20.1 K with a relative standard deviation of 23-32%. This increase in temperature due to indirect heating caused by the warm room, might thus be sufficient to prevent condensation within the sampling line. Higher ΔT were measured by both TSI3565 and AURORA3000 nephelometers behind the WAI-2 in period D and E, with mean values of 25.2 K (± 22%) 25.9 K (± 25%), respectively.

Considering humidity, int_RH remained below the 40% mark during 93% of the time between 2007 and 2023. During the Period A, B and C, RH_{SL} exceeded 40% for 1%, 3% and 11% of time, respectively. It is important to note that RH_{SL} values above 40% were never recorded by both TSI3565 and AURORA3000 nephelometers behind the WAI-2 in period D and E, when the mean RH_{SL} was 14% and 18% respectively. As shown in Figure S3b, the air reaching the end of the sampling line dries considerably with respect to ambient conditions. In the absence of an heated inlet head, ΔRH was -40% in Period A. After the upgrade to WAI-1 without a direct drying system, the mean ΔRH varied from -54% during Period B to -49% in period C. However, it must be noted that during the longest sampling periods (B and C), 60 and 1289 hourly ΔRH positive values where observed in Period B (less than 0.2% of the time and ΔRH up to +25%) and C (2.1% of the time and ΔRH up to +45%), respectively. These peculiar “humidity-enrichment” events mostly occurred during daytime, in cloud-free conditions and at ambient RH levels below 60%. For the overall period, $RH_{SL\text{-}A}$ remained below 40% during 43% of RH-enriched hours, while higher $RH_{SL\text{-}A}$ were observed 57% of the time. We did not observe any correlation or convolution with pressure, wind speed, wind direction or temperature.

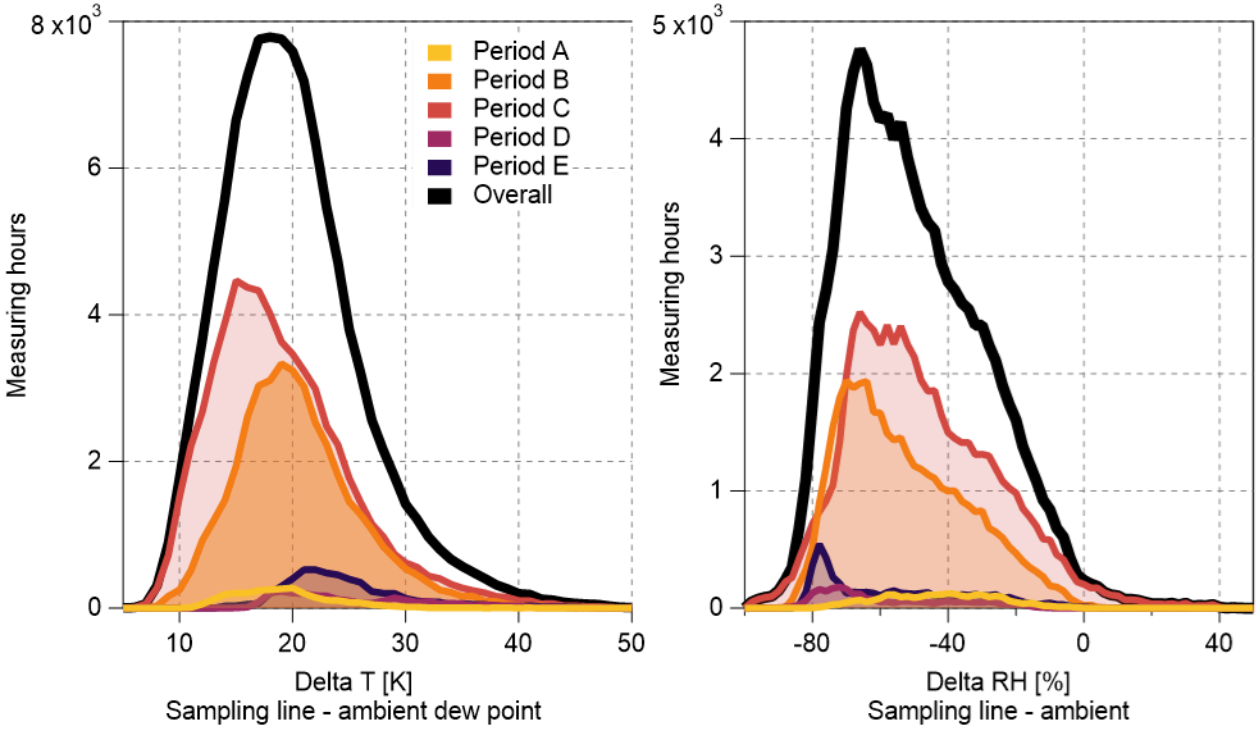

Figure S3 Comparison of ambient conditions and conditions in the sampling line: a) histogram of temperature difference between the inlet line and the ambient dew point temperature; b) histogram of the relative humidity difference between the sampling line and the ambient. Period A: downward looking inlet and M9003 nephelometer, 2007-2007. Period B: whole air inlet 1 M9003 nephelometer, 2007-2023. Period C: whole air inlet 1 and TSI3565 nephelometer, 2014-2022. Period D: whole air inlet 2 and TSI3565 nephelometer, 2022-2023. Period E: whole air inlet 2 and AURORA3000 nephelometer, 2023-2024.

S3. Comparison between nephelometer and line-sensor measurements

In this section we compare the temperature and humidity measurements performed via the nephelometers at the end of the sampling line with the one performed with the dedicated sensors inside the sampling line after the dryer and before the nephelometer. Due to adjustment and testing of the inlet line and acquisition software, the line-sensor were available only for the year 2023 with a limited temporal coverage (183 valid measurement days), including the last month of Period D (28 days, nephelometer model TSI3565) and the first months of Period E (161 days, nephelometer model AURORA3000). First, the T_{SL} showed a high correlation between the nephelometers and the line-sensors (r^2>0.97; Figure S4a). In both periods, warmer temperatures were recorded by the nephelometers, with temperature dependent offset during period D (slope of the fitted line of 0.79) and an apparent constant offset during Period E (slope of the fitted line of 0.96). As shown in Figure S4c, the temperature measured at the end of the line was overestimated by 4.3 K (IQR = 4.8 – 4.1 K) with the nephelometer TSI3565 and by 6.6K (IQR = 6.7-6.4 K) with ARUORA3000 nephelometer. Although RH_{SL} showed a high correlation between the nephelometers and the line-sensor (r^2>0.98; Figure S4b), both nephelometer showed a slope slower than unity compared to the line-sensor. As shown in Figure S4d, the resulting RH offset of the nephelometer with respect to the line-sensor, in the 0-40% RH range, was quantified to be negative in Period D (Median = -4.3 %; IQR = -4.3 – -8.4 %) and null in Period E (Median = 0.10 % ; IQR = 1.3 – -1.2 %).

Overall, conditions at the end sampling line observed with the various nephelometer from 2007 to 2023 might not accurately represent the actual conditions inside the sampling line. Hence, the air in main inlet line and in the MAAP sampling line might be colder by 4-7 K and more humid by 0-6%.

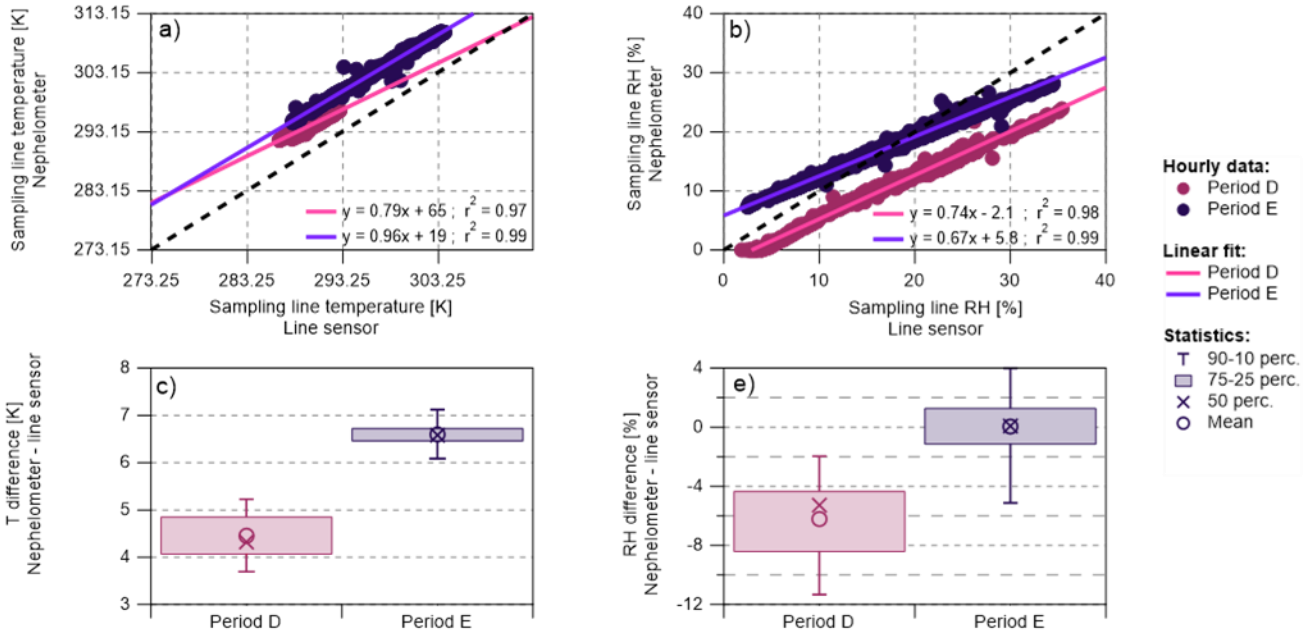

Figure S4 Comparison of temperature and relative humidity measured at the end of the sampling line with nephelometers and in the sampling line sensors.

S4. eBC-dataset application with ERA5 data

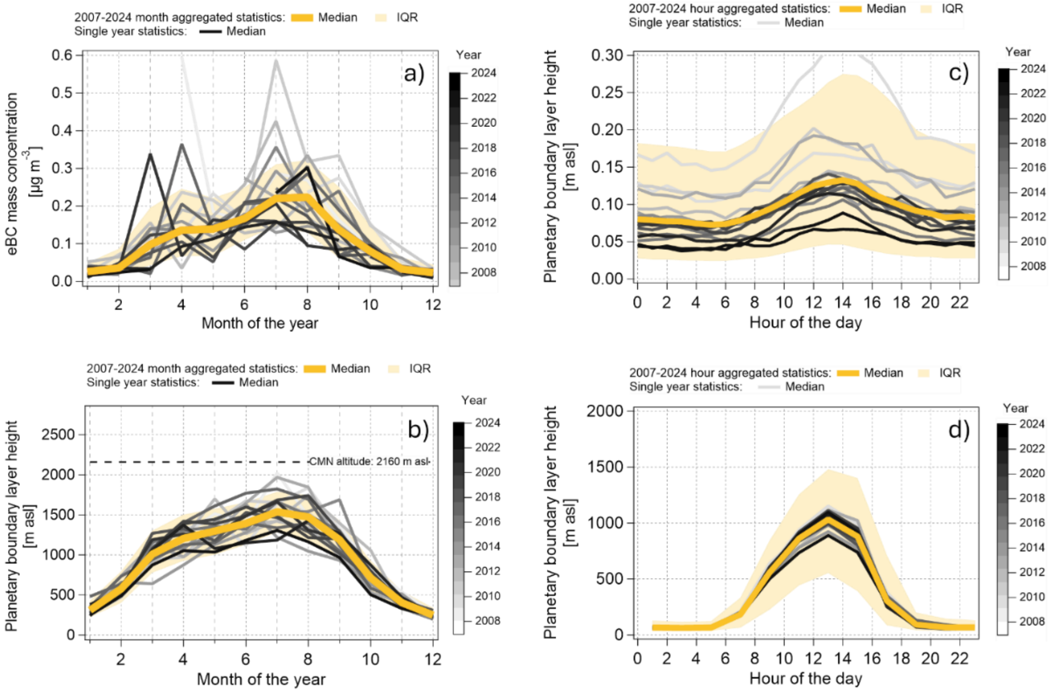

Figure S 5 Seasonal (a,b) and daily (c,d) cycle of equivalent black carbon (eBC) mass concentration measured at Cimone and planetary boundary layer height derived from ERA-5 reanalysis data. Statistic calculated based observations at CMN between 2007 and 2023.

S5. eBC-dataset application with FLEXPART products and their description

The FLEXPART products used in this work are accessed through the ACTRIS data portal, which provides a range of black carbon (BC) diagnostics. The interface allows users to select the station, time period (year and month), product type, and spatial projection (regional, global, polar), and to navigate through individual time steps. Data can be visualized online or downloaded in netCDF (map-based products) or ASCII format (time series products). The products can be grouped into three main categories: transport diagnostics and time resolved attribution.

The Footprint product ("*Footprint*") represents emission sensitivity, indicating the probability that emissions from a given region contribute to concentrations at the receptor site over a 30-day backward simulation. Time-resolved source attribution include the source type attribution ("*Source Spec*"), emission continent area attribution ("*Continent Spec*") and atmospheric ageing time ("*Age Spec*").

"Source Spec" products describe the contribution of different emission sources to BC concentrations, including residential and commercial combustion (DOM BC), energy production (ENE BC), industrial processes (IND BC), gas flaring (FLR BC), shipping (SHP BC), waste treatment (WST BC), transportation (TRA BC), and open biomass burning (Fire BC). These products are based on ECLIPSEv6 emissions (Klimont et al., 2017) and GFEDv4 for biomass burning (Giglio et al., 2013). The Total BC product, used int the present study, represents the sum of all contributions, its hourly and monthly variability is

compared with the eBC observations in Figure S 6. “*Continent Spec*” provides information on the regional origin of BC: OCE: Ocean, GNL: Greenland, SA: South America, CA: Central America, NA: North America, AFR: Africa, EUR: Europe, RUS: Russia, ASI: Asia excluding Russian part, AUS: Australia). “*Age Spec*” quantify the age contribution of the plume to surface BC, indicating how “fresh” or “aged” the air arriving at the receptor is.

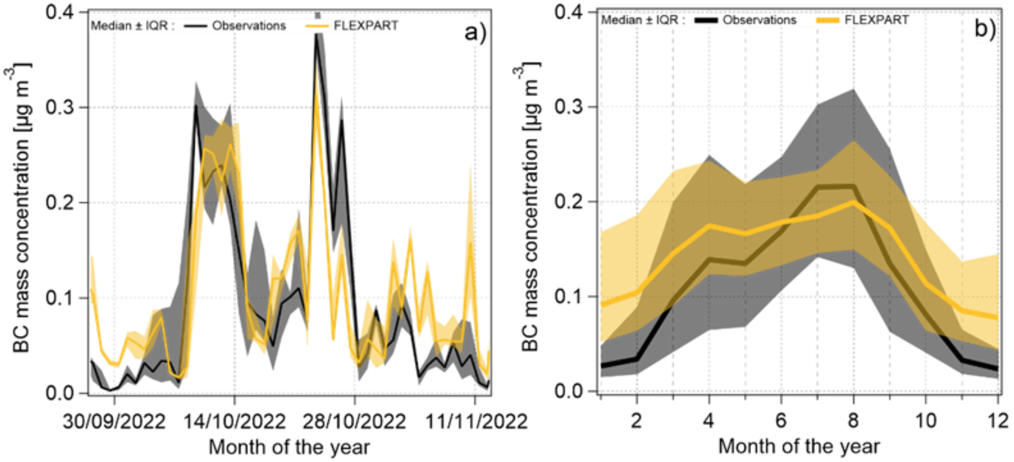

Figure S 6 Comparison between observations and FLEXPART simulations of black carbon BC mass concentration at daily (a) and seasonal (b) temporal resolution.